ResearchGate

See discussions, stats, and author profiles for this publication at: https://www.researchgate.net/publication/233934099

Neogene–Recent extension on the eastern flank of Mount Olympus, Greece

Article *in* Tectonophysics · June 2010

DOI: 10.1016/j.tecto.2009.05.011

CITATIONS
12

READS
274

1 author:

R. Damian Nance
Ohio University
198 PUBLICATIONS **5,912** CITATIONS

SEE PROFILE

Some of the authors of this publication are also working on these related projects:

Cornish beam engines View project

All content following this page was uploaded by R. Damian Nance on 08 October 2017.

The user has requested enhancement of the downloaded file.

Tectonophysics 488 (2010) 282–292

Contents lists available at ScienceDirect

Tectonophysics

journal homepage: www.elsevier.com/locate/tecto

Neogene–Recent extension on the eastern flank of Mount Olympus, Greece ☆

R. Damian Nance *

Department of Geological Sciences, 316 Clippinger Laboratories, Ohio University, Athens, Ohio 45701, USA

ARTICLE INFO

Article history:
Received 14 May 2008
Received in revised form 10 December 2008
Accepted 18 May 2009
Available online 29 May 2009

Keywords:
North Aegean
Mount Olympus
Extensional exhumation
Uplift rates
Neotectonics

ABSTRACT

The Olympus massif of NE Greece comprises metamorphosed and deformed Triassic and Cretaceous–Eocene carbonates considered to represent part of the passive southwestern margin of Neotethys, which separated the Apulia plate of mainland Greece from southern Europe in the Mesozoic. Ocean closure in the Early Tertiary led to subduction of this passive margin, as a result of which the Olympus carbonates were tectonically overridden in the Eocene by a series of thrust sheets consisting of locally high P/T (blueschist) metamorphosed continental margin sediments, basement granitoid gneisses, and ophiolitic rocks.

Following collision, uplift of the Olympus carbonates by ~6–8 km was accomplished by Early Neogene ductile and Late Neogene–Recent brittle normal faulting, which exposed the carbonates in the form of a structural window through the overriding thrust stack. The focus of this exhumation occurred on the eastern flank of the massif where a thick calc–mylonite with down-to-the-east sense-of-shear indicators and a prominent zone of NNW- to NW-trending brittle normal faults separate the carbonates from telescoped structurally overlying units. Published $^{40}Ar/^{39}Ar$ microcline ages that indicate a thermal perturbation close to the contact zone in excess of 100–150 °C at 16–23 Ma (Early Miocene) are taken to date the onset of ductile extension, and imply long-term uplift rates of ~0.4 to 1 km/m.y.

Degradation of Pleistocene glacial features on the Olympus massif and the presence on its eastern piedmont of deeply incised streams, erosional terraces, and fault scarps that offset the sedimentary deposits of three cycles of Pleistocene glacial deposition (Units 1–3), testify to its continuing uplift. A prominent frontal fault offsets Unit 2 by >150 m and several subsidiary NW-trending normal faults with a cumulative displacement of ~130 m offset a paleosol developed on Unit 1. Kinematic indicators indicate normal dip-slip movement. Cumulative fault displacement for Unit 1 exceeds 277 m, yielding a minimum uplift rate of ~1.3 mm/yr, given the oxygen isotope stage 7 (Mindel/Riss) age of 210 ka proposed for the Unit 1 paleosol. Cumulative offset of >196 m for the paleosol developed on Unit 2 yields an uplift rate of ~1.6 mm/yr, given its proposed isotope stage 5e (Riss/Würm) age of 125 ka. This estimate is supported by longitudinal valley profile data that document ~200 m of stream incision since Unit 2 deposition and show the offset as reflecting uplift of the Olympus massif rather than subsidence of the adjacent Gulf of Thermaikos. Assuming 1.8 Ma for the base of the Pleistocene, these rates yield a total uplift range for the Quaternary of 2.3–4.1 km, consistent with the present 2.6 km height of Olympus above the exposed frontal fault.

Neogene uplift of Olympus was likely facilitated by extension accompanying the opening of the Aegean back-arc basin during the Miocene as a result of the southward retreat of the Hellenic subduction zone. For the Pliocene–Recent, uplift was likely facilitated by extension linked to the termination of dextral motion at the western end of the North Anatolian Fault associated with the westward tectonic escape of Anatolia.

© 2009 Elsevier B.V. All rights reserved.

1. Introduction

The northern Aegean Sea and its continental borders form an area of critical importance to studies of the geological evolution of the eastern Mediterranean, both in regard to the region's complex history of subduction and collision during the Mesozoic–Cenozoic (e.g., Schmitt, 1983; Schermer, 1990, 1993; Schermer et al., 1990; Lips et al., 1998; Ricou et al., 1998; Brown and Robertson, 2004; Sharp and Robertson, 2006; Lacassin et al., 2007) and to its more recent history of extension and transtension (e.g., Jackson, 1994; Kilias et al., 2002; Mountrakis, 2006) that is geodynamically linked to the roll-back of the Hellenic arc and to the ongoing indentation of the Arabian plate (Fig. 1). This latter history has been the product of complex tectonic interactions governed largely by the interplay of a succession of tectonic regimes: (1) gravitational collapse of previously thickened crust as a result of back-arc extension associated with the southward retreat of the Hellenic arc from the Oligocene to middle Miocene (e.g., Le Pichon and Angelier, 1979; Mercier et al., 1989; Gautier et al., 1999; Jolivet and Faccenna, 2000), (2) westward escape of Anatolia (Turkey) since the late Miocene as a consequence of the ongoing collision

☆ Tectonophysics manuscript number: TECTO6226.

* Tel.: +1 740 593 1107; fax: +1 740 593 0486.
E-mail address: nance@ohio.edu.

0040-1951/$ – see front matter © 2009 Elsevier B.V. All rights reserved.
doi:10.1016/j.tecto.2009.05.011

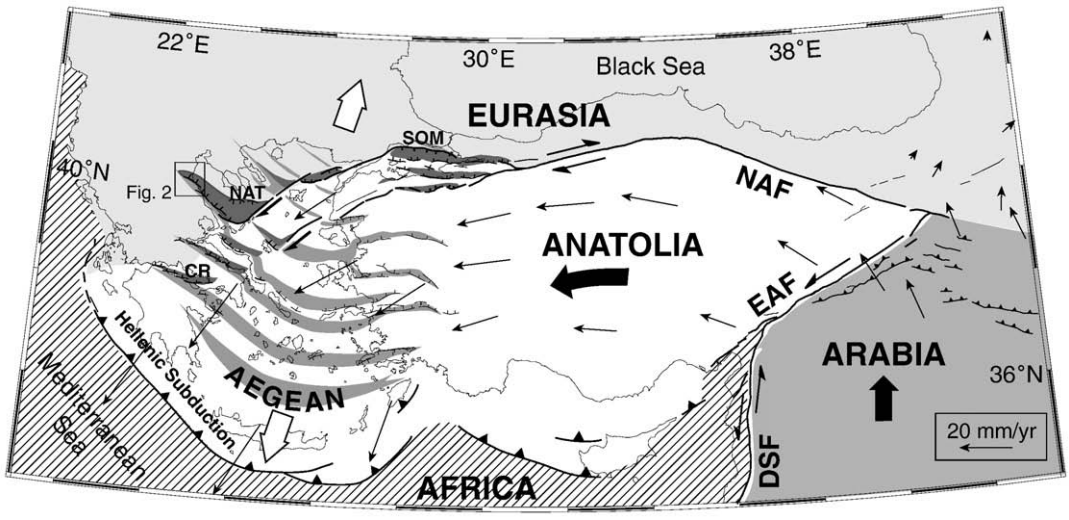

Fig. 1. Tectonic setting of continental extension in the Aegean Sea (after Armijo et al., 1999), in which active right–lateral motion and local, rapid, post-Late Pliocene westward propagation of the North Anatolian Fault (NAF) associated with the westward escape of Anatolia from the Arabia–Eurasia collision zone (curved black arrow), is superimposed on slower Oligocene–middle Miocene back-arc extension (grey stripes and white arrows) associated with the southward retreat of the Hellenic arc, and has successively opened the pull-apart and rift basins (in dark grey) of the Sea of Marmara (SOM), the North Aegean Trough (NAT), and the Corinth Rift (CR). Current velocity vectors relative to Eurasia (in mm/yr) from Reilinger et al. (1997). EAF = East Anatolian fault, DSF = Dead Sea fault. Box identifies location of Fig. 2.

between the Arabian and Eurasian plates (e.g., Taymaz et al., 1991; Dinter and Royden, 1993; Le Pichon et al., 1995; Saatçilar et al., 1999; Dinter, 1998; Mantovani et al., 2006), and (3) westward propagation of the dextral North Anatolian Fault, which accommodates this escape, into the northern Aegean since the Late Pliocene (e.g., Armijo et al., 1999; Flerit et al., 2004; McNeill et al., 2004).

Although the effects of these tectonic interactions occur largely in the offshore realm, details of the geometry, kinematics and current horizontal motion of the individual crustal blocks involved (Fig. 1) have been relatively well constrained on the basis of seismic and bathymetric surveys (e.g., Lyberis, 1984; Mascle and Martin, 1990; Lykousis, 1991; Piper and Perissoratis, 1991; Laigle et al., 2000; Koukouvelas and Aydin, 2002; Papanikolaou et al., 2006), and from geodetic surveys employing global positioning and satellite laser ranging (e.g., Reilinger et al., 1997; Cocard et al., 1999; McClusky et al., 2000; Kreemer et al., 2004). Less well known are the effects of these complex motions on the extent and timing of extension on individual faults, and the consequent rates of uplift and subsidence of the regions they border. In northern mainland Greece, for example, the outcome of these tectonic interactions has been one of simple extension, much of which has been localized along large, inherited faults that have transected northern Greece since the Oligocene. As a result, it is along some of these faults that much of the widespread present-day seismic activity in the region is focused (e.g., Mountrakis et al., 2006).

One such fault forms the eastern boundary of the Olympus massif, which rises abruptly from the western margin of the Gulf of Thermaikos in the northern Aegean Sea (Fig. 2), and is home to the highest mountain in Greece (2917 m). This fault forms part of a range-bounding system (Fig. 3) that extends northwest and southeast to border the eastern margins of the High Pieria mountains and Ossa massif, respectively, and records a protracted ductile to brittle evolution that spans more than 20 million years. As a result, it affords a unique opportunity to examine the rates of normal fault movement at very different scales and over very different time frames — those averaged over the history of extension in kilometers per million years (km/m.y.), and those determined from the recent geologic past in millimeters per year (mm/yr). The influence of normal fault movement on morphological features of Pleistocene to Recent fluvio–glacial activity also allows extension as a consequence of down-throw of the hanging wall to be distinguished from that associated with up-throw of the footwall. This article reviews the extensional history of the eastern margin of the Olympus massif, and the data on which it is based, in order to place constraints on the quantification of these variables.

2. Geologic setting

Mount Olympus in Greece is a massive, uplifted plateau of Triassic and Lower Cretaceous to Eocene shelf limestones (Fig. 3) that are considered to represent the passive southwestern margin of the Mesozoic Neotethys Ocean (e.g., Schermer, 1990; Mountrakis, 2006), and which are overlain by Eocene siliciclastic rocks (flysch) deposited at the onset of ocean closure. These units are presently exposed in the form of a tectonic window through a series of thrust sheets that were tectonically emplaced onto the parautochthonous carbonate platform and flysch in the Late Eocene (e.g., Godfriaux, 1968; Barton, 1976; Schmitt, 1983; Schermer et al., 1990; Lips et al., 1998) as the Neotethys Ocean closed and its southwestern continental margin was subducted beneath southern Europe on the overriding plate. Most recent studies show these thrusts to be west-vergent (e.g., Schermer, 1993; Brown and Robertson, 2004), although opposing views exist in the early literature (e.g., Barton, 1975; Nance, 1981) and conflicting tectonic models variably place the collisional suture in the Vardar Zone to northeast of the Olympus massif (e.g., Schermer, 1990; Sharp and Robertson, 2006) or in the Pindos Zone to the southwest (e.g., Papanikolaou, 1984, 2009; Mountrakis, 2006).

Four major thrust units are recognized in the area surrounding Mount Olympus (Schermer et al., 1990): (1) the structurally lowest Ambelakia Unit comprising continental margin quartzofeldspathic metasedimentary and minor mafic to intermediate metavolcanic rocks locally metamorphosed at high P/T (blueschist facies) in the Paleogene and Eocene, (2) the Pierien and (3) Infrapierien Units comprising deformed Paleozoic basement gneisses and granites overlain by Permian–Triassic metasedimentary and metavolcanic rocks and Triassic–Jurassic platform carbonates, and (4) dismembered ophiolitic rocks of probable Middle Jurassic age (Vergely, 1976) that form the structurally highest unit (Fig. 4).

As a result of post-collisional uplift, the focus of which has occurred on the eastern side of the massif, each of these thrust units now outcrops in a more-or-less concentric arrangement on the flanks of the Olympus plateau (Fig. 3). A similar disposition of units occurs around the parautochthonous platform carbonates and Eocene flysch

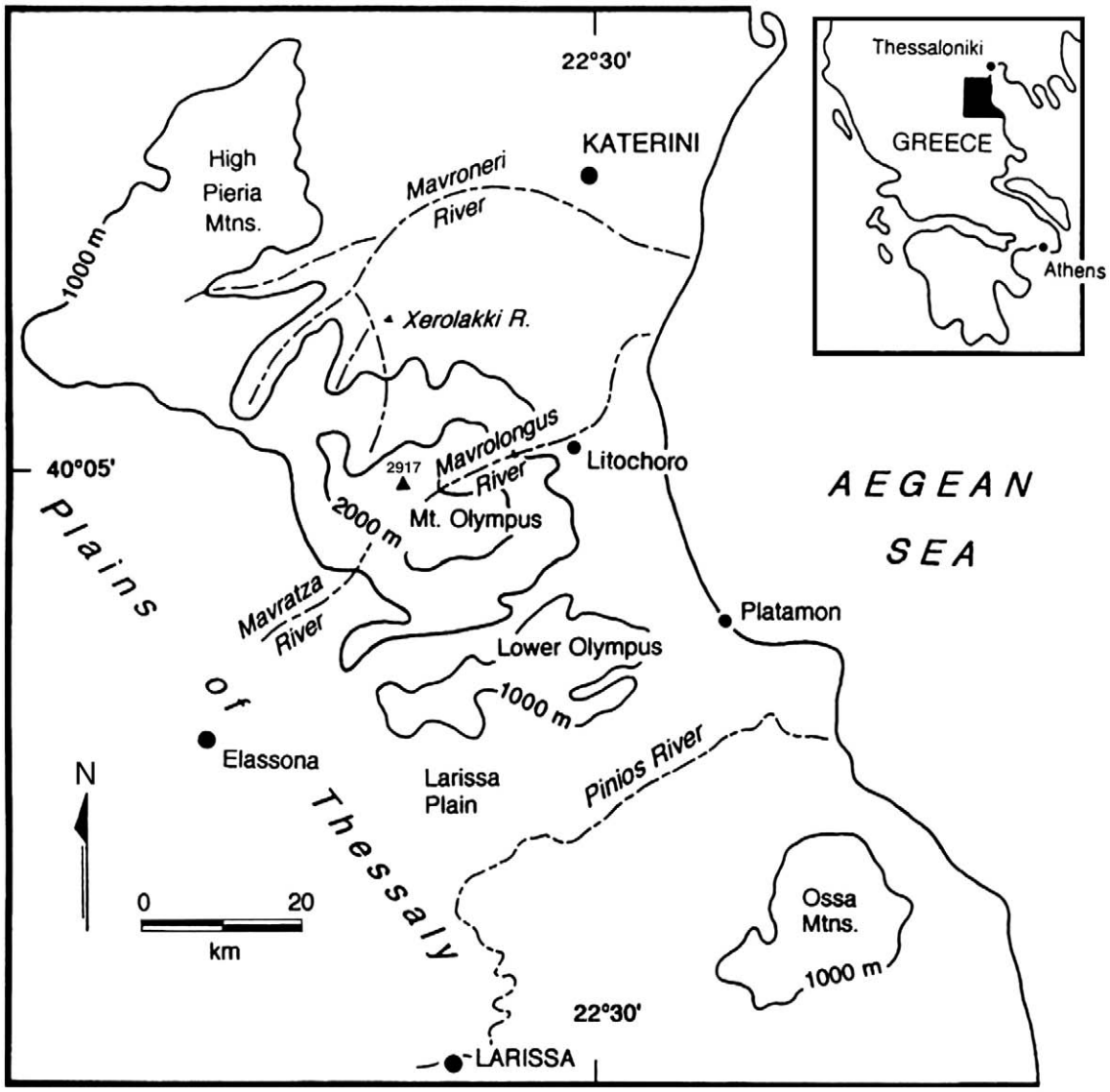

Fig. 2. Geographic map of the Olympus region of northeastern mainland Greece showing major towns and rivers. The Mavrolongus becomes the Enipeas River upon reaching the coastal plain (see Fig. 1 and inset for location).

of the Ossa tectonic window to the southeast (e.g., Schmitt, 1983; Lips et al., 1998), whereas the High Pieria mountains to the northwest are underlain by Late Paleozoic granites and metamorphic rocks (e.g., Yarwood and Aftalion, 1976; Nance, 1981; Kotopouli et al., 2000).

During the Pleistocene, uplift of the Olympus plateau was concomitant with glacial activity, three cycles of which have been identified on the basis of sedimentary deposits on its eastern and western piedmont (e.g., Faugères, 1977; Psilovikos, 1984; Smith et al., 1997, 2006). Each of the three sedimentary deposits (Units 1–3; Fig. 5) can be related to features of glacial erosion on the plateau upland and are separated by prominent soil horizons (paleosols) that record interstadial or interglacial intervals and can be correlated with a succession of dated soils (Demitrack, 1986) on the southern side of the Olympus massif (Smith et al., 1997). This correlation suggests that the oldest and most significant glacial advance (Unit 1) corresponds to the Mindel glaciation in the Olympus region during marine isotope stage (MIS) 8 at ca. 260,000 years before present (BP), and that subsequent stages of deposition (Units 2 and 3) record glacial activity on the plateau during the Riss (MIS 6) glaciation at ca. 160,000 years BP, and the Würm (MIS 4–2) glaciation between 70,000 and 20,000 years BP (e.g., Imbrie et al., 1984), respectively. Uplift of the plateau along its eastern flank concomitant with these glacial cycles has led to the development on its eastern piedmont of deeply incised streams, erosional terraces and fault scarps that offset all three sedimentary units of glacial deposition (Fig. 6). It is this range-front fault zone and the record it provides of the uplift history of the Olympus plateau in response to regional extension within the northern Aegean that forms the focus of this study.

3. Record of extension

Uplift of the Olympus carbonates, which followed terminal collision in the Eocene, has been largely accomplished by Early Neogene ductile shearing (e.g., Schermer et al., 1990) and Late Neogene to Recent brittle faulting along the massif's eastern flank (e.g., Smith et al., 1997). The range-front fault zone that has accommodated this movement comprises several hundred meters of calc–mylonite, a prominent NNW-trending brittle normal fault, and a series of subsidiary NW–SE normal faults that, together, have brought the parautochthonous platform carbonates of the Olympus plateau into tectonic juxtaposition with ophiolitic rocks of the uppermost thrust unit.

The range-front fault zone can be traced for more than 20 km, but is best exposed where it crosses the Mavrolongus–Enipeas valley in

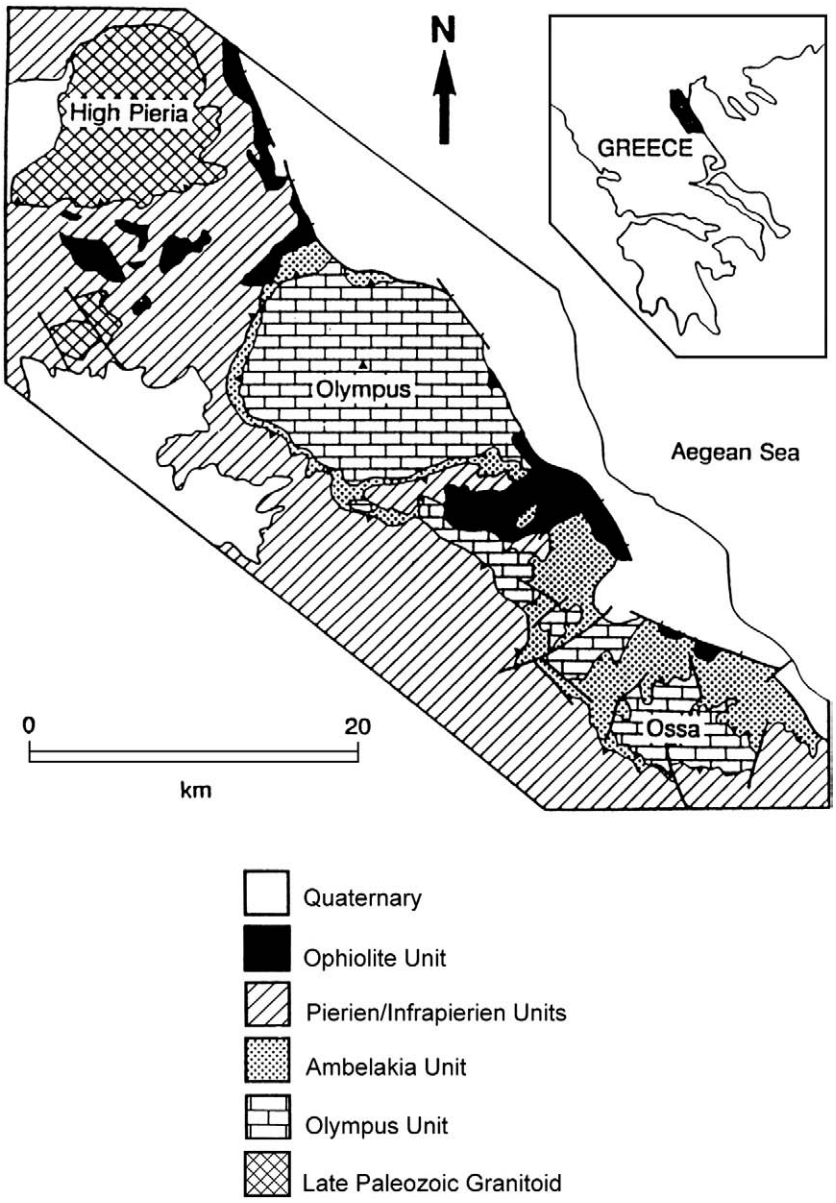

Fig. 3. Generalized tectonic map of the Mount Olympus region from Smith et al. (1997), simplified after Yarwood and Aftalion (1976), Nance (1981), Schmitt (1983), Katsikatsos and Migiros (1987) and Schermer et al. (1990). Olympus Unit = Triassic and Cretaceous to Early Tertiary shelf carbonates; Ambelakia Unit = Mesozoic continental margin sediments; Pierian and Infrapierian Units = Paleozoic metamorphic rocks and granites; Ophiolite Unit = dismembered ophiolitic rocks. Normal faults with ticks on downthrown side, thrust faults with black triangles on hangingwall. Inset shows location.

the vicinity of the town Litochoro (Fig. 6). At Milos, a kilometer west of the town, the main frontal fault comprises a pair of east-dipping normal faults that cross cut a thick zone of calc–mylonites developed within the carbonates of the Olympus massif and juxtapose these mylonites against serpentinites and mica schists that represent telescoped sections of the structurally overlying units (Fig. 7a). Northeast of the town, the fault zone continues with a series of smaller piedmont faults that cross cut the present-day Enipeas alluvial fan developed between the uplifted mountain front and the coastline of the Aegean Sea.

3.1. Ductile extension: fabrics, age and displacement

The earliest fabrics within the frontal fault zone are those of ductile deformation and take the form of a strong mylonitic foliation that contains a well-defined down-dip (east-plunging) calcite stretching lineation. Centimeter-scale, rusty weathering dolomitic pods within the calcite mylonitic fabric define σ-structures that indicate normal (down-to-the-east) motion during ductile shear.

The timing of this extensional mylonitization can be constrained by examining published $^{40}Ar/^{39}Ar$ thermochronology (Schermer et al., 1990). Phengites obtained from two mica schists of the Pierien Unit lying structurally above the extensional mylonite zone on the southern flank of Olympus have yielded relatively simple age gradients from 65 Ma to 40 Ma, with ~60% of the gas released in the 50–60 Ma range, and from a near plateau age of 58.7 ± 1.9 Ma to 42 Ma, respectively. Microclines from the same samples show saddle-shaped profiles with high-temperature increments that level off at ca. 50–55 Ma and minimum ages in the range 16–23 Ma.

Coupled with $^{40}Ar/^{39}Ar$ data obtained from the Pierien and Infrapierien units on the western flank of the Olympus plateau, these ages have been interpreted to record three thermal events during which the argon system was perturbed (Schermer et al., 1990): (1) an event at ca. 53–61 Ma (Middle Paleocene–Early Eocene; Gradstein et al., 2004) defined by the high-temperature increments in

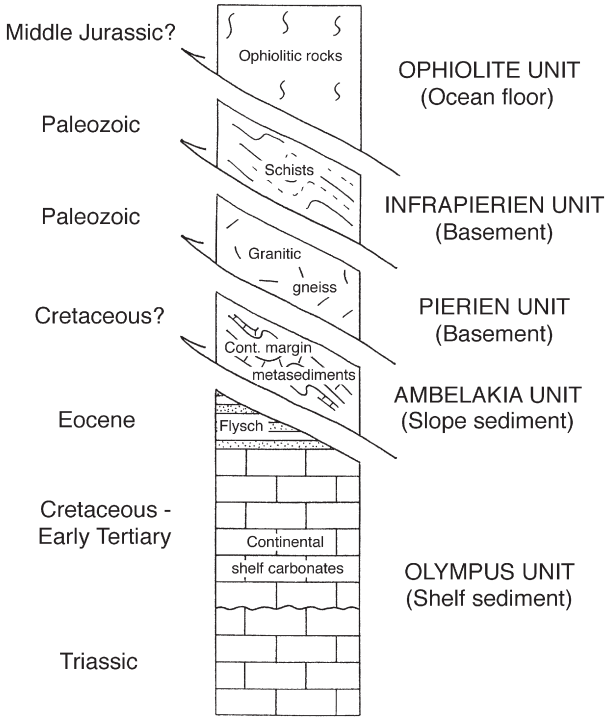

Fig. 4. Structural stacking inferred for the Olympus massif (after Schermer et al., 1990). The parautochthonous platform carbonates and Eocene flysch of the Olympus Unit are presently exposed in the form of a tectonic window through the overriding thrust sheets, the emplacement of which occurred in the Late Eocene. Figure not to scale but minimum structural thickness of allochthonous units estimated to be 6–8 km (Schermer, 1990).

phengite, (2) an event at ca. 36–40 Ma (Middle–Late Eocene; Gradstein et al., 2004) defined by the low-temperature increments in phengite, and (3) an event at ca. 16–23 Ma (Early Miocene; Gradstein et al., 2004) defined by the minimum ages of microcline. The first two events accompanied deformation and metamorphism above the closure temperature of phengite at ~350–400 °C (e.g., Dahl, 1996; McDougall and Harrison, 1999) and are attributed to convergent tectonic processes. The first thermal event is interpreted to record continental (A-type) subduction and high-pressure blueschist facies metamorphism of the basement and continental margin units concomitant with the closure of the Neotethys Ocean, whereas the second event is taken to date final thrusting of the blueschists over the Olympus carbonate platform. The former is consistent with $^{40}Ar/^{39}Ar$ evidence for high-pressure metamorphism and exhumation at ca. 54 Ma in the Ossa massif (Lips et al., 1998), whereas the latter is supported by a Rb–Sr whole rock age of 39 ± 1 Ma on phyllonites from the Olympus thrust zone on the western flank of the plateau that is likewise taken to date emplacement of allochthonous units over the parauthochthonous Olympus platform (Barton, 1976). The age of this event in the Ossa massif has been placed at ca. 45 Ma (Lips et al., 1998).

The third thermal event at ca. 16–23 Ma, however, accompanied deformation but no metamorphic mineral growth (Schermer et al., 1990) and is interpreted to record the onset of post-collisional uplift and cooling associated with normal fault movement and the development of the tectonic window and present-day Olympus plateau. Similar $^{40}Ar/^{39}Ar$ white mica ages of 15–27 Ma from mylonites in the Pelion range, on-strike to the southeast of the Olympus–Ossa massifs, are likewise attributed to extensional ductile shear (mostly towards to northeast) and are interpreted to record crystallization below the white mica closure temperature (Lips et al., 1999; Lacassin et al., 2007).

In the Olympus massif, any deformation associated with this event took place above the closure temperature of microcline at ~100–150 °C (Harrison and McDougall, 1982; McDougall and Harrison, 1999), but below that of phengite, which records no perturbation of argon systematics at this time. These temperatures would have been insufficient to produce mylonitic fabics in the predominantly quartzofeldspathic rocks of the Pierien and Infrapierien Units, but would have been capable of producing calc–mylonites in the Olympus carbonates, given the significantly lower brittle–ductile transition temperature for calcite (150–250 °C; e.g., Kennedy and White, 2001) relative to that of quartz (300–350 °C; e.g., Evans et al., 1990). Hence, the minimum $^{40}Ar/^{39}Ar$ ages defined by microcline (ca. 16–23 Ma) are taken to date the formation of the calc–mylonite within the frontal fault zone, thereby placing the onset of ductile extension on the eastern flank of the Olympus plateau in the Early Miocene.

If this is the case, minimum estimates of displacement and displacement rate can be derived from the offset across the calc–mylonite zone, which separates parautochthonous carbonates of the Olympus massif from serpentinites of the uppermost allochtononous unit. Field mapping of the eastern and western flanks of the Olympus massif (e.g., Barton, 1975; Schmitt, 1983; Latsoudas, 1985; Katsikatsos and Migiros, 1987; Schermer, 1990) suggests that the minimum

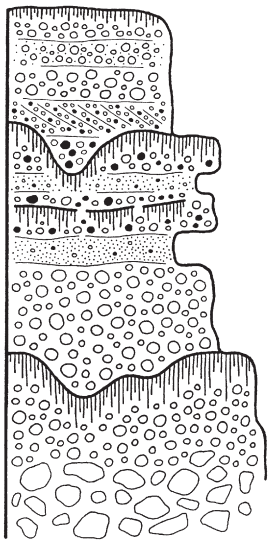

Thin chocolate brown (or red brown) soil.
(MODERN NON-GLACIAL Weathering)

UNIT 3 Uniform, non-lithified, well-sorted, clast- and matrix-supported, stratified gravel and sand. Erosional basal contact. Surface terraced and faulted.
(Predominantly PROGLACIAL OUTWASH)

Thick brown (upper) and red brown (lower) soils in upper part of unit.
(INTERGLACIAL/INTERSTADIAL Weathering)

UNIT 2 Non-uniform, lithified and non-lithified, clast- and matrix-supported, stratified gravel, sand and pebbly silt. Erosional basal contact. Locally terranced. Faulted.
(PROGLACIAL OUTWASH AND ALLUVIAL FAN)

Thick, red, clay-enriched soil at surface
(INTERGLACIAL Weathering)

UNIT 1 Uniform, lithified, predominantly matrix-supported diamict and gravel. Basal contact not observed. Faulted.
(GLACIAL DIAMICT, PROGLACIAL OUTWASH)

Fig. 5. Generalized Quaternary stratigraphy of the eastern piedmont of the Olympus massif showing the three depositional units (Units 1–3) linked to glacial activity on the plateau, their character and interpretation, and the major soil horizons that separate them (after Smith et al., 1997). Not to scale.

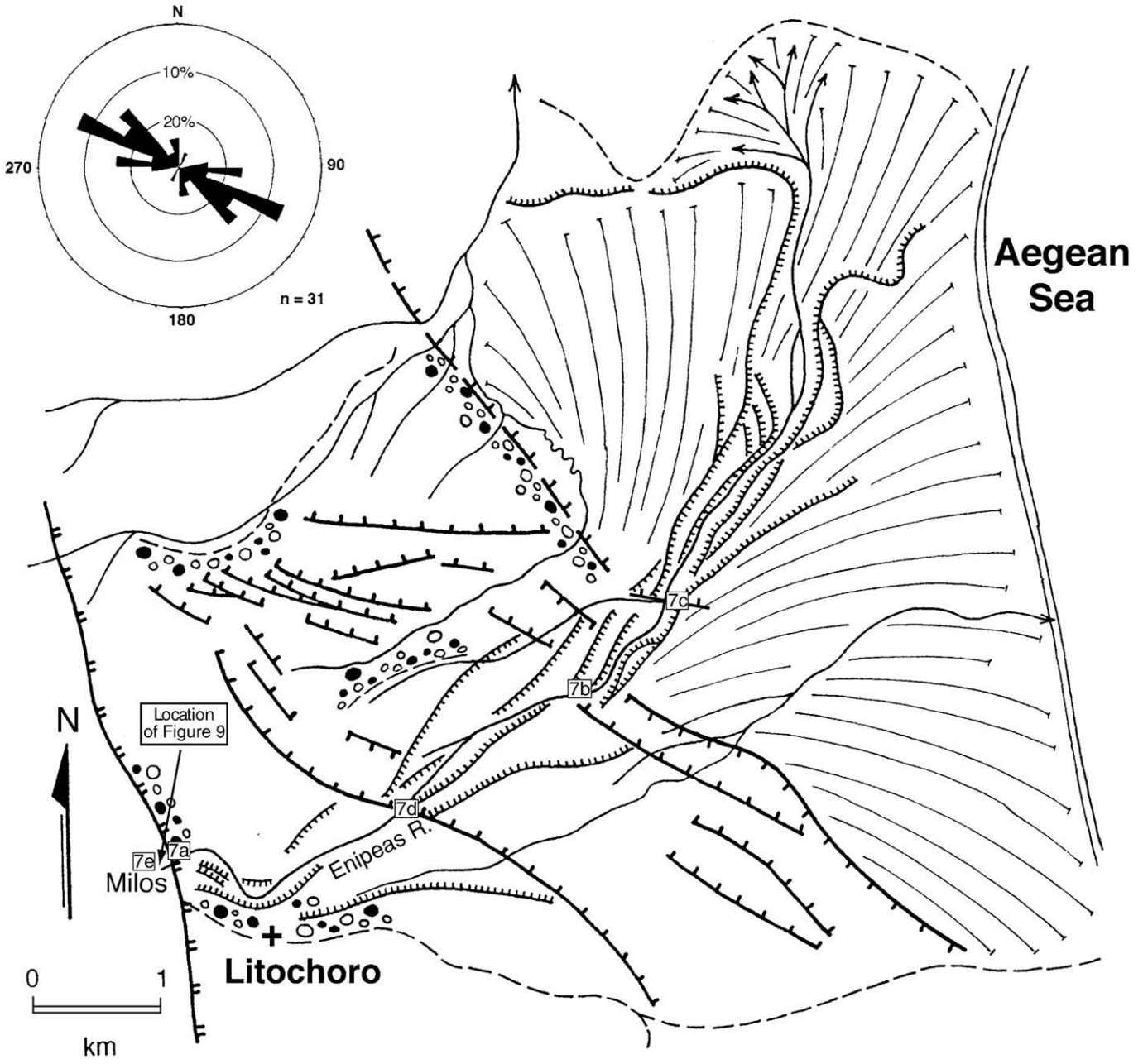

Fig. 6. Geomorphological map (based on field mapping, aerial photographs and 1:50,000 topographic control) of the eastern piedmont of the Olympus plateau in the vicinity of Litochoro at the mouth of the Mavrolongus gorge (modified from Smith et al., 2006). Dashed lines delimit the Litochoro alluvial fan; fine lines show form of fan surface; fine-toothed lines represent fluvial terraces bordering the Mavrolongus–Enipeas river (flow indicated by arrows); pebble pattern shows distribution of Unit 1 glacial diamict; and heavy lines identify faults offsetting piedmont surface with ticks on downthrown side (main frontal fault lies west of Litochoro). Inset shows rose diagram of fault trends. Numbers in boxes locate photographs shown in Fig. 7.

structural thickness of the allochtonous units transported across the Olympus platform prior to its uplift is 6–8 km. Given continuous uplift since its onset, this would require a long-term linear uplift rate of ~0.38 km/m.y. since the Early Miocene.

A similar estimate can be derived from the thermal offset represented by the calc–mylonite zone, which juxtaposes unmetamorphosed carbonates against quartzofeldspathic schists of the Pierien Unit that experienced temperatures in excess of 350–400 °C at ca. 36–40 Ma. Assuming a geothermal gradient of 25 °C/km, these temperatures correspond to depths of 14–16 km, requiring a long-term linear uplift rate of ~0.4 km/m.y. since the Late Eocene if uplift was continuous.

These rates are likely to be seriously underestimated since both would be significantly increased if the uplift of the Olympus plateau was episodic rather than continuous. For example, ductile extension that was confined to the Early Miocene would increase the first estimate by a factor of more than 2.5 (to ~1 km/m.y.).

3.2. Brittle extension: features, age and offsets

The transition from ductile to brittle extension in the Olympus region is of uncertain timing but likely occurred during the mid- to Late Miocene, assuming cooling rates of ~10 °C/Ma (Schermer et al., 1990) following the Early Miocene thermal event. Fault offsets of deposits linked to glacial activity show that all movements have been brittle since the onset of Pleistocene glaciation.

The focus of this brittle motion has been on the main NNW-trending frontal fault (Fig. 7a), although subsidiary NW–SE to WNW–

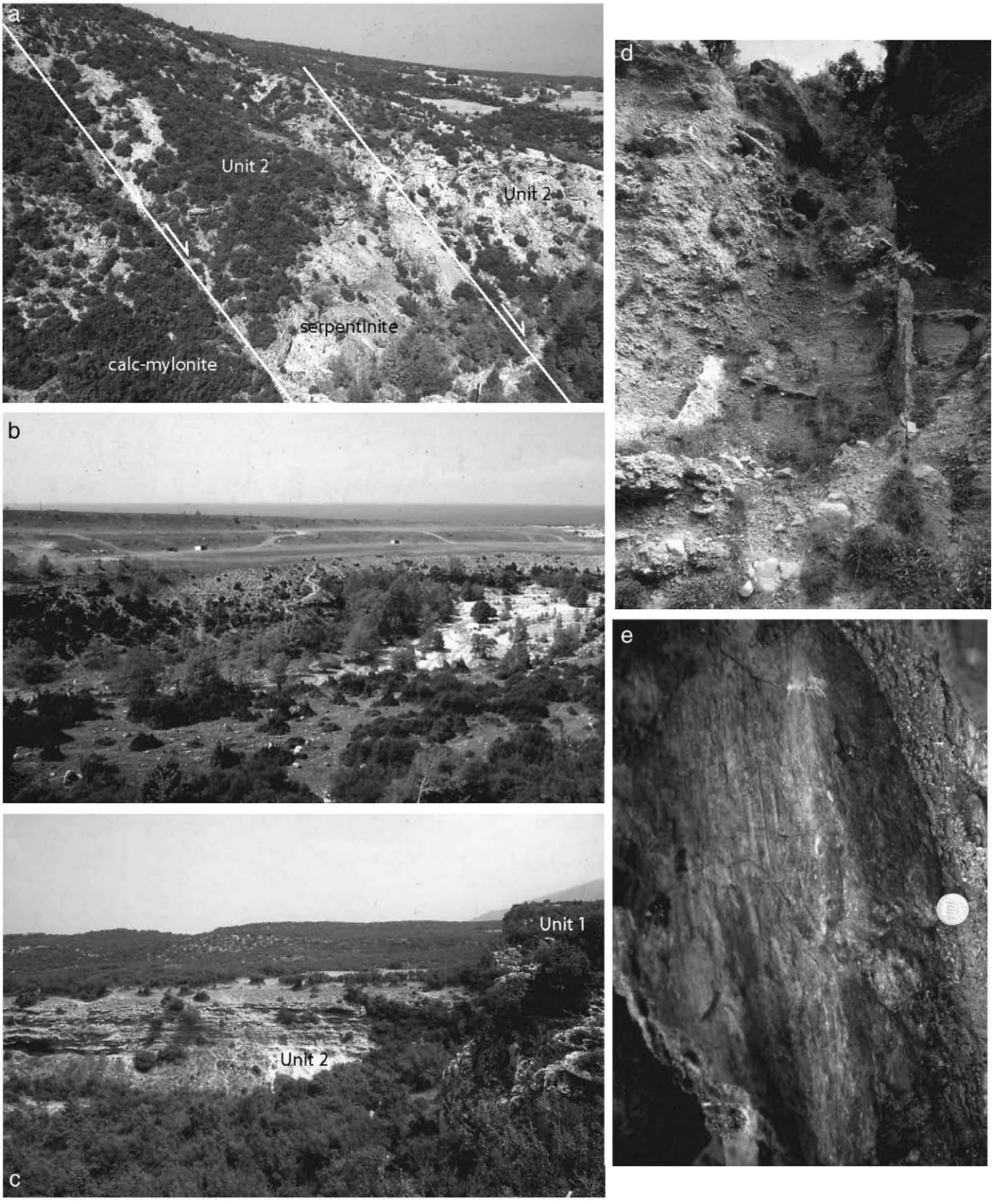

Fig. 7. Field photographs of extensional features on the eastern piedmont of the Olympus massif (see Fig. 6 for locations). (a) Main frontal fault viewed north across the Mavrolongus gorge at Milos, immediately west of Litochoro. Fault segments juxtapose calc–mylonites developed within parautochthonous carbonates of the Olympus Unit from serpentinites of the structurally highest allochthonous unit, both of which are overlain by offset sediments of Unit 2. (b) Stream terraces developed in unconsolidated sediments of Unit 3 adjacent to the Enipeas River (foreground) northeast of Litochoro. (c) Piedmont fault scarp separating fully lithified sediments of Unit 1 from partially lithified sediments of Unit 2 on the Enipeas alluvial fan northeast of Litochoro (Fault 4; Fig. 8). (d) Calcified fault breccia developed in sediments of Unit 3 exposed where piedmont fault (Fault 1; Fig. 8) crosses the Enipeas River northeast of Litochoro. (e) Down-dip striations developed in serpentinite adjacent to main frontal fault in the Mavrolongus gorge at Milos, immediately west of Litochoro. Photographs by J. McIntyre.

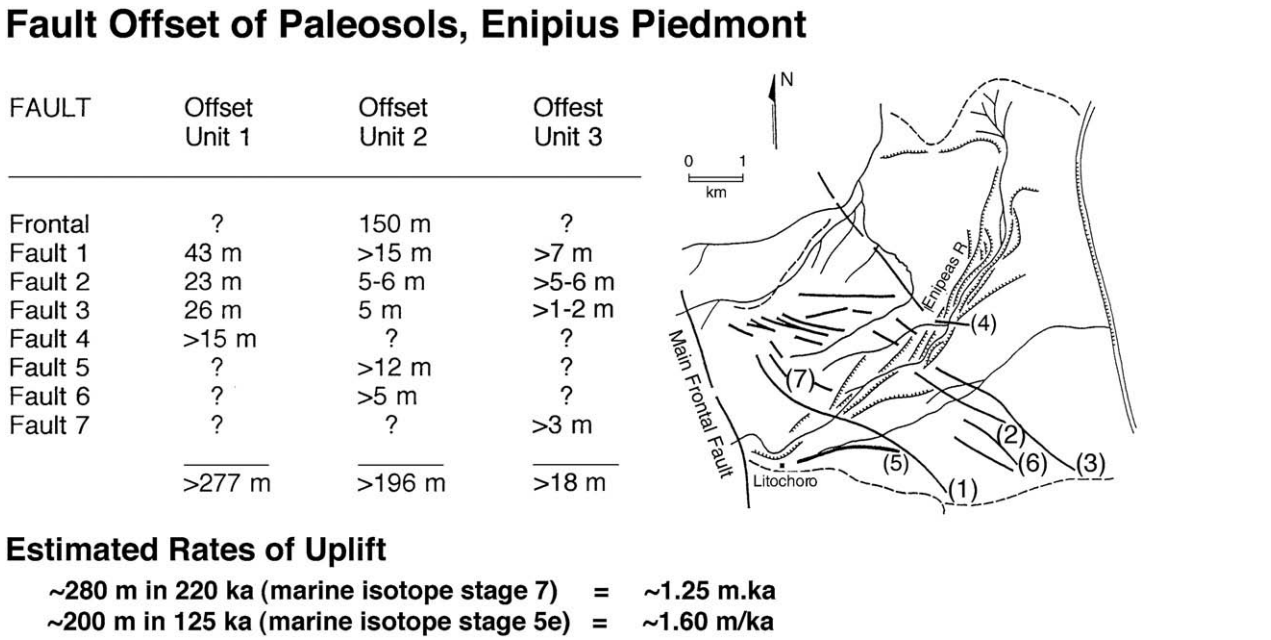

Fig. 8. Summary of the amount of offset of soils and paleosols developed on sediments of Units 1–3 measured across the main frontal fault and subsidiary faults (1–7) on the eastern piedmont of the Olympus massif at Litochoro (from Smith et al., 2006).

ESE faults that offset Quaternary deposits on the eastern piedmont show that uplift has occurred over a broad zone of fault movement several kilometers in width (Fig. 6). This splay-like arrangement is interpreted to imply that the main frontal fault is of listric geometry and is intersected by the piedmont faults at depth. Uplift across this broad fault zone has significantly degraded the erosional features of Pleistocene glaciation on the Olympus massif (Smith et al., 1997) and has resulted in the creation of deeply incised streams, erosional terraces (Fig. 7b), and fault scarps (Fig. 7c) that offset the sedimentary deposits of each of the three cycles of Pleistocene glacial deposition (Units 1–3). These features provide various criteria by which the amount and rate of uplift during the Quaternary can be estimated.

The main frontal fault consists of two segments, several hundred meters apart, which separate serpentinized ophiolitic rocks of the uppermost allochthonous unit from mylonitic carbonates of the Olympus platform (Fig. 7a), a structural omission of 6–8 km (e.g., Schermer, 1990). The faults, which trend 170/70E at Milos, also separate partially lithified piedmont sediments of Unit 2 from those of the Olympus massif with a minimum offset of 150 m (Fig. 8), 17 m of which occurs across the more eastern of the two fault segments. The paleosol developed on Unit 2 is also offset across the subsidiary faults of the piedmont fan by at least another 46 m, giving a minimum offset across the frontal fault zone of 196 m since the Unit 2 paleosol formed. Additional downcutting by the Mavrolongus–Enipeas river through the sedimentary base of the Unit 2 deposits on the downthrown side of the main frontal fault at Milos amounts to at least 25 m (Fig. 9), and is taken to reflect stream incision in response to faulting on the piedmont fan following the deposition of Unit 3.

The piedmont faults, the longest of which (Fault 1; Fig. 8) can be traced for more than 3 km, form a series of fault scarps that offset the modern surface of the Enipeas alluvial fan (Fig. 6). These piedmont faults are younger than, and oblique to, the main frontal fault and trend predominantly NW–SE to WNW–ESE (inset Fig. 8). Where exposed, they are marked by fault breccias and gouge (Fig. 7d) developed in the sediments of Units 1–3, and shown down-dip striations (Fig. 7e) with kinematic indicators consistent with normal dip-slip movement. In addition to recording a cumulative offset of the Unit 2 paleosol of almost 50 m, seven of these faults collectively displace the paleosol developed on Unit 1 by more than 127 m, and the modern soil on Unit 3 by at least 18 m (Fig. 8). The total offset of the Unit 1 paleosol across the frontal fault zone therefore amounts to at least 277 m.

In addition to using measured fault offset data, estimates of uplift rates can be determined from the influence of these offsets on stream incision. As a result of displacements across the frontal fault zone, the longitudinal profile of the Mavrolongus–Enipeas River is interrupted by prominent breaks or knickpoints (Fig. 10). These abrupt changes in stream gradient are produced when episodes of faulting cause renewed stream incision in response to the change in baseline. Downcutting above the site of fault displacement causes the knickpoint to progressively migrate upstream as the channel attempts to re-establish a new graded profile.

The Mavrolongus–Enipeas profile shows two prominent knick points, which are thought to reflect offset on the main frontal fault and piedmont faults, respectively (Fig. 10). Projection of the valley profile above the upper knickpoint to the present day coastline suggests that upwards of 200 m of stream incision has occurred in response to offset on the main frontal fault since the development of the soil profile on Unit 2. Projection to the coast of the longitudinal profile above the lower knickpoint suggests that ~30 m of this stream incision post-

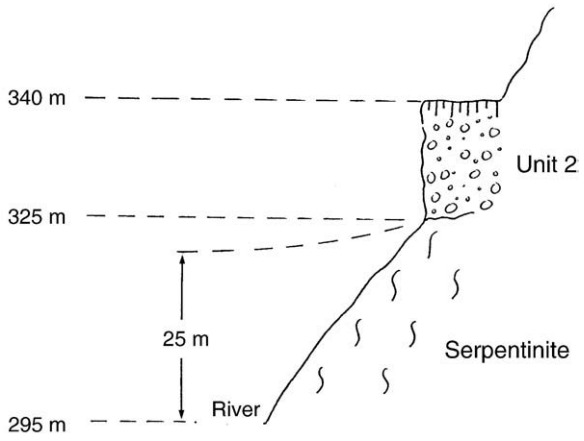

Fig. 9. Field sketch of stream incision through Unit 2 deposits in the Mavrolongus gorge on the downthrown side of the main frontal fault at Milos. See Fig. 6 for location.

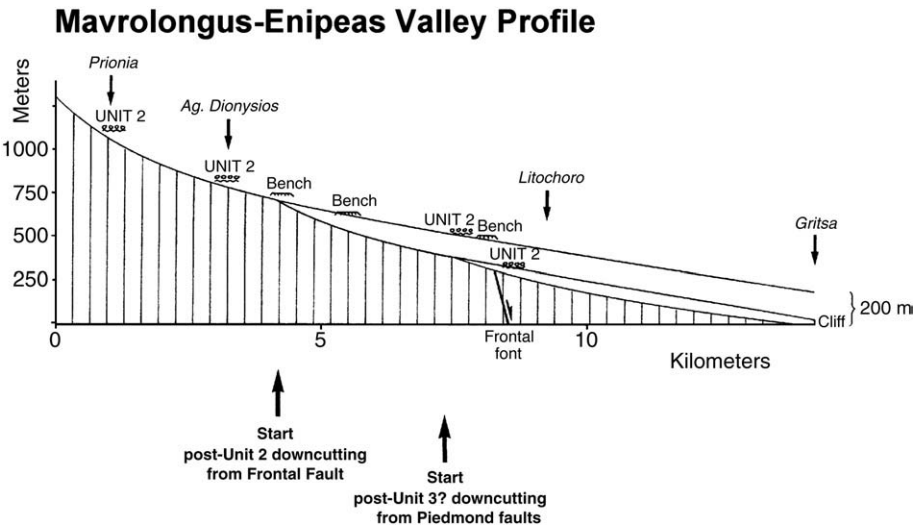

Fig. 10. Longitudinal profile (based on 1:50,000 topographic coverage) of the entire length of the Mavrolongus–Enipeas valley (see Figs. 2 and 6) showing heights of Unit 2 deposits, topographic benches, and nick points used to estimate uplift rates during the Quaternary (from Smith et al., 2006). Longitudinal profiles extended to the coast at Gritsa from each nick point approximate valley profiles prior to each episode of renewed river incision.

dates the deposition on Unit 3 and occurred in response to fault movement on the piedmont.

Based on these measurements, several estimates can be made of the rate of fault movement since the soils formed on each of the three piedmont sedimentary units. For example, the minimum cumulative offset of the Unit 1 paleosol across the frontal fault zone of >277 m (Fig. 8) yields a minimum rate of movement of ~1.3 mm/yr, assuming a marine isotope stage (MIS) 7 (Mindel/Riss) age of ca. 210 ka (e.g., Imbrie et al., 1984) for the development of this interglacial feature. Conversely, the cumulative offset of >196 m for the paleosol developed on Unit 2 yields an uplift rate of ~1.6 mm/yr, assuming a MIS 5e (Riss/Würm) age of ca. 125 ka for this paleosol. This latter estimate is supported by the Mavrolongus–Enipeas valley profile, which records ~200 m of stream incision since the deposition of Unit 2 (Fig. 10). Importantly, this incision further confirms that all fault offsets since the deposition of Unit 2 reflect uplift of the Olympus massif rather than subsidence of the adjacent Gulf of Thermaikos. The valley profile also indicates stream incision of ~30 m as the result of fault offset since the deposition of Unit 3, a figure supported by the amount of post-Unit 2 downcutting (>25 m) by the Mavrolongus–Enipeas river evident on the downthrown side of the main frontal fault at Milos (Fig. 9). Assuming a MIS 2 (Würm) age of ca. 20 ka for the upper limit of Unit 3 deposition, this yields an uplift rate of at least ~1.5 mm/yr. Measured fault offsets on the piedmont suggest that >18 m of this uplift occurred on piedmont faults.

These estimates, the most reliable of which is considered to be that recorded by the uplift of Unit 2 (~1.6 mm/yr) because it is supported by two independent measurements, suggest that uplift of the Olympus plateau has occurred at a relatively uniform rate for at least the past 200,000 years. If an age of 1.81 Ma is used for the start of the Pleistocene (Gradstein et al., 2004), these values can be extrapolated to produce a range of total uplift for the Quaternary of 2.3–2.9 km, which is in keeping with the present topographic elevation of Mount Olympus above the frontal fault zone of ~2.6 km.

4. Discussion

Uplift of the Olympus massif, based on structural offset and topographic relief, amounts to more than 10 km, and has been largely accomplished by Miocene ductile and Plio–Pleistocene brittle displacement along it eastern flank. Rates of uplift range from ~0.4 to 1.0 mm/yr (~0.4–1 km/m.y.) for ductile movement and ~1.3–1.6 mm/yr during brittle faulting. The estimates for Quaternary uplift are generally consistent with those of Faugères (1977), Schermer et al. (1990) and Stiros et al. (1994) and, on the basis of steam incision, can be shown to reflect uplift of the Olympus plateau rather than subsidence of the Gulf of Thermaikos.

Whether this history, which spans more than 20 million years, reflects discrete episodes of extension or more-or-less continuous uplift under decreasing pressure–temperature conditions is uncertain and, in the absence on the eastern piedmont of exposed sediments older than Unit 1, rates of brittle displacement for the Plio–Pleistocene cannot be estimated. Nevertheless, the rates of long-term and short-term uplift are similar, and the strike of the mylonitic fabric developed during the ductile phase of deformation is parallel to that of the main brittle frontal fault, suggesting that both developed in response to an extension direction of the same (ENE–WSW) orientation. This is consistent with observations in the Pelion range, on-strike to the southeast of the Olympus–Ossa massifs, where offshore normal faults and tension gashes lying perpendicular to an extensional stretching lineation plunging broadly NE (050°) suggest that the direction of extension remained the same as deformation evolved from ductile to brittle (Lips et al., 1999; Lacassin et al., 2007).

However, paleomagnetic data for the western Aegean (van Hinsbergen et al., 2005) show that mainland Greece rotated 40° clockwise between 15–13 Ma and 8 Ma in response to the southward retreat of the Hellenic arc, and has rotated clockwise an additional 10° since 4 Ma as a consequence of strike-slip faulting associated with the westward escape of Anatolia, which is accommodated in the northern Aegean by the dextral North Anatolian Fault (Fig. 1). Hence, prior to this rotation, the extension direction recorded in the orientation of the calc–mylonite stretching lineation and the strike of the main frontal fault would have been closer to NNE–SSW, an orientation consistent with extension accompanying the roll back of the Hellenic subduction zone.

The orientation of the younger faults on the Olympus piedmont (Fig. 6), on the other hand, suggests that a change in the direction of extension to one of broadly NE–SW orientation followed the development of the main frontal fault. This orientation matches the extension direction associated with the opening of the North Aegean Trough as a result of the westward propagation of the dextral North Anatolian Fault into the northern Aegean (Fig. 1). Hence, the orientation of the piedmont faults is thought to record the change in extension accompanying the switch in tectonic regime from that associated with the retreat of the Hellenic arc to that accompanying the westward propagation of the North Anatolian Fault.

Interestingly, although many of the faults of the frontal fault zone offset modern surfaces and, hence, have been recently active, none are associated with historical or instrumental seismicity (e.g., Hatzfeld, 1999). Hence, they are not included among the seismically active faults of northern Greece (Mountrakis et al., 2006). This apparent seismic inactivity may indicate a recurrence interval on these faults that is longer than the observational record (~100 years) or, if the younger piedmont faults sole into the main frontal fault at depth, as is thought to be the case, it may reflect transfer of movement away from the main frontal fault as its orientation has become increasingly oblique to the present direction of extension, which is linked to the westward propagation of the North Anatolian Fault. As a result, extensional motion may have been taken up by more favorably oriented, NW–SE faults such as those of the piedmont and those bordering the North Aegean Trough (e.g., Papanikolaou et al., 2006).

5. Conclusions

The structural architecture of the Olympus region, in which Mesozoic–Early Tertiary platform carbonates of the Olympus and Ossa massifs outcrop in the form of tectonic windows through an overriding stack of thrust sheets emplaced in the Late Eocene, reflects a history of post-collisional uplift and extension that has been largely accomplished by normal faulting along the eastern flank of the massifs. Examination of the frontal fault zone of the Olympus massif, coupled with previously published age data, shows that this post-collisional extension has spanned an interval of more than 20 million years, was responsible for uplift in excess of 10 km, and records the following sequence of events:

(1) An early phase of ductile deformation and calc–mylonite formation that took place at temperatures between 150 °C and 300 °C and began in the Early Miocene (ca. 16–23 Ma; Schermer et al., 1990). Ductile extension likely terminated in the mid- to Late Miocene and was associated with kinematic indicators that document normal dip-slip movement toward the present-day east.
(2) A subsequent phase of Plio–Pleistocene brittle normal faulting that was responsible for the formation of the NNW-trending main frontal fault.
(3) A final phase of Pleistocene to Recent brittle faulting responsible for the formation of the NE–SW to ENE–WSW faults of the Olympus piedmont.

In the absence of uplift data for the Plio–Pleistocene, it is uncertain whether these phases were continuous or episodic.

Estimates of the rate of uplift during the ductile phase of extension range from 0.4 to 1 km/m.y., whereas those estimated from fault offsets and stream incision and their effects on longitudinal stream gradients, suggest minimum uplift rates of ~1.3–1.6 mm/yr during the most recent (Middle–Late Pleistocene) phase of brittle normal faulting. These estimates imply 2.3–4.1 km of uplift for the Quaternary consistent with the present 2.6 km topographic elevation of the Olympus carbonates above the exposed frontal fault.

Taking into account the clockwise rotation of mainland Greece by 40° during the interval 15–8 Ma, and the additional 10° of clockwise rotation since 4 Ma, a change in the direction of extension from broadly north–south to NE–SW following the development of the main NNW-trending frontal fault is indicated by the change in strike of the younger NW- and WNW-trending piedmont faults. These orientations suggest that the Early Neogene uplift of the Olympus massif (and the concomitant subsidence of the Gulf of Thermaikos) was likely facilitated by extension accompanying the opening of the Aegean back-arc basin during the Miocene as a result of the southward retreat of the Hellenic subduction zone. For the Pliocene–Recent, on the other hand, uplift was likely facilitated by extension linked kinematically to termination of dextral motion at the western end of the North Anatolian Fault associated with the westward tectonic escape of Anatolia.

Acknowledgements

Funding for this project was provided by the National Geographic Society, the Earthwatch Center for Field Research, and Ohio University. For field assistance and support in Greece, the author is indebted to Jay McIntyre (Ohio University), Giorgos Papathanasiou and the Satrazemis family (Litochoro), and Kostas Zolotas (Olympus). Constructive comments by A.G. Smith and two anonymous reviewers greatly improved the original manuscript.

References

Armijo, R., Meyer, B., Hubert, A., Barka, A., 1999. Westward propagation of the North Anatolian Fault into the northern Aegean; timing and kinematics. Geology 27, 267–270.
Barton, C.M., 1975. Mount Olympus, Greece: new light on an old window. J. Geol. Soc. Lond. 131, 389–396.
Barton, C.M., 1976. The tectonic vector and emplacement age of an allochthonous basement slice in the Olympos area, N.E. Greece. Bull. Soc. Geol. France 18, 253–258.
Brown, S.A.M., Robertson, A.H.F., 2004. Evidence for Neotethys rooted within the Vardar suture zone from the Voras Massif, northernmost Greece. Tectonophys. 381, 143–173.
Cocard, M., Kahle, H.G., Peter, Y., Geiger, A., Veis, G., Felekis, S., Paradissis, D., Billiris, H., 1999. New constraints on the rapid crustal motion of the Aegean region: recent results inferred from GPS measurements (1993–1998) across the West Hellenic Arc, Greece. Earth Planet. Sci. Let. 172, 39–47.
Dahl, P.S., 1996. The crystal–chemical basis for Ar retention in micas; inferences from interlayered partitioning and implications for geochronology. Contribs. Mineral. Petrol. 123, 22–39.
Demitrack, A., 1986. The late Quaternary geologic history of the Larissa plain, Thessaly, Greece: Tectonic, climatic, and human impact on the landscape [Ph.D. dissert.]: Stanford, California, Stanford University, 134 p.
Dinter, D.A., 1998. Late Cenozoic extension of the Alpine collisional orogen, northeast Greece: origin of the north Aegean basin. Geol. Soc. Amer. Bull. 110, 1208–1230.
Dinter, D.A., Royden, L., 1993. Late Cenozoic extension in northeastern Greece: Strymon Valley detachment system and Rhodope metamorphic core complex. Geology 21, 45–48.
Evans, B., Fredrich, J.T., Wong, T.-F., 1990. The brittle to ductile transition in rocks: recent experimental and theoretical progress. In: Duba, A.G., Durham, W.B., Handin, J.W., Wang, H.F. (Eds.), The brittle–ductile transition — The Heard Volume: Geophys. Monogr. Ser., 56, pp. 1–20.
Faugères, L., 1977. Naissance et dévelopment du relief de l'Olympe (Grèce). Revue de Géographie Physique et de Géologie Dynamique 19 (2), 7–26.
Flerit, F., Armijo, R., King, G., Meyer, B., 2004. The mechanical interaction between the propagating North Anatolian Fault and the back-arc extension in the Aegean: Earth Planet. Sci. Lett. 224, 347–362.
Gautier, P., Brun, J.P., Moriceau, R., Sokoutis, D., Martinod, J., Jolivet, L., 1999. Timing, kinematics and cause of Aegean extension: a scenario based on a comparison with simple analogue experiments. Tectonophys. 315, 31–72.
Godfriaux, I., 1968. Étude géologique de la région de l'Olympe. Annales Géologiques des Pays Helléniques, 19, pp. 1–284.
Gradstein, F.M., Ogg, J.G., Smith, A.G., Bleeker, W., Lourens, L.J., 2004. A new geologic time scale, with special reference to Precambrian and Neogene. Episodes 27, 83–100.
Harrison, T.M., McDougall, I., 1982. The thermal significance of potassium feldspar K–Ar ages inferred from $^{40}Ar/^{39}Ar$ age spectrum results. Geochim. Cosmochim. Acta 46, 1811–1820.
Hatzfeld, D., 1999. The present-day tectonics of the Aegean as deduced from seismicity. In: Durand, B., Jolivet, L., Horvath, F., Seranne, M. (Eds.), The Mediterranean Basins, tertiary extension within the Alpine Orogen: Geol. Soc. Spec. Publ. London, 156, pp. 417–426.
Imbrie, J., Hays, J.D., Martinson, D.G., McIntyre, A., Mix, A.C., Morley, J.J., Pisias, N.G., Prell, W.L., Shackleton, N.J., 1984. The orbital theory of Pleistocene climate: support from a revised chronology of the marine delta^{18}O record. In: Berger, A.L., Imbrie, J., Hays, J., Kukla, G., Saltzman, B. (Eds.), Milankovitch and Climate, Part 1. InReidel Publishing Company, Dordrecht, pp. 269–305.
Jackson, J., 1994. Active tectonics of the Aegean region. Ann. Rev. Earth and Planet. Sci. 22, 239–271.
Jolivet, L., Faccenna, C., 2000. Mediterranean extension and the Africa–Eurasia collision. Tectonics 19, 1095–1106.
Katsikatsos, G., Migiros, G., 1987. Geological map of Greece, Rapsani sheet: Athens, Greece, Institute of Geology and Mineral Exploration, scale 1:50 000.
Kennedy, L.A., White, J.C., 2001. Low-temperature recrystallization in calcite: mechanisms and consequences. Geology, 29, 1027–1030.
Kilias, A.A., Tranos, M.D., Orozco, M., Alonso-Chaves, F.M., Soto, J.I., 2002. Extensional collapse of the Hellenides: a review: Revista de la Sociedad Geológica de España, 15, pp. 129–139.
Koukouvelas, I., Aydin, A., 2002. Fault structure and related basins of the North Aegean Sea and its surroundings. Tectonics 21, 1046. doi:10.1029/2001TC901037.

Kotopouli, C.N., Pe-Piper, G., Piper, D.J.W., 2000. Petrology and evolution of the Hercynian Pieria Granitoid Complex (Thessaly, Greece): paleogeographic and geodynamic implications. Lithos 50, 137–152.
Kreemer, C., Chamot-Rooke, N., Le Pichon, X., 2004. Constraints on the evolution and vertical coherency of deformation in the Northern Aegean from a comparison of geodetic, geologic and seismologic data. Earth Planet. Sci. Lett. 225, 329–346.
Lacassin, R., Arnaud, N., Leloup, P.H., Armijo, R., Meyer, B., 2007. Syn- and post-orogenic exhumation of metamorphic rocks in North Aegean. eEarth, 2, 51–63.
Laigle, M., Hirn, A., Sachpazi, M., Roussos, N., 2000. North Aegean crustal deformation: an active fault imaged to 10 km depth by reflection seismic data. Geology, 28, 71–74.
Latsoudas, Ch., 1985. Geological map of Greece, Kantariotissa–Litochoro sheet. Athens, Greece, Institute of Geology and Mineral Exploration, scale 1:50 000.
Le Pichon, X., Angelier, J., 1979. The hellenic arc and trench system: a key to the neotectonic evolution of the eastern Mediterranean area. Tectonophysics 60, 1–42.
Le Pichon, X., Chamot-Rooke, N., Lallemant, S., Noomen, R., Veis, G., 1995. Geodetic determination of the kinematics of central Greece with respect to Europe: implications for eastern Mediterranean tectonics. J. Geophys. Res. 100, 612675–612690.
Lips, A.L.W., White, S.H., Wijbrans, J.R., 1998. $^{40}Ar/^{39}Ar$ laserprobe dating of discrete deformational events: a continuous record of early Alpine tectonics in the Pelagonian Zone, NW Aegean area, Greece. Tectonophys. 298, 133–153.
Lips, A.L.W., Wijbrans, J.R., White, S.H., 1999. New insights from $^{40}Ar/^{39}Ar$ laserprobe dating of white mica fabrics from the Pelion Massif, Pelagonian Zone, internal Hellenides, Greece; implications for the timing of metamorphic episodes and tectonic events in the Aegean region. In: Durand, B., Jolivet, L., Horvath, F., Seranne, M. (Eds.), The Mediterranean Basins, tertiary extension within the Alpine Orogen: Geol. Soc. Spec. Publ. London, 156, pp. 457–474.
Lyberis, N., 1984. Tectonic evolution of the North Aegean trough. In: Dixon, J.E., Robertson, A.H.F. (Eds.), The geological evolution of the Eastern Mediterranean: Geol. Soc. Lond. Spec. Publ., 17, pp. 709–726.
Lykousis, V., 1991. Sea-level changes and sedimentary evolution during the Quaternary in the northwest Aegean continental margin, Greece. Int. Assoc. Sedimentologists Spec. Publ., 12, pp. 123–131.
Mantovani, E., Viti, M., Babbucci, D., Tamburelli, C., Albarello, D., 2006. Geodynamic connection between the indentation of Arabia and the Neogene tectonics of the central-eastern Mediterranean region. In: Dilek, Y., Pavlides, S. (Eds.), Postcollisional Tectonics and Magmatism in the Mediterranean region and Asia: Geol. Soc. Amer. Spec. Pap., 409, pp. 15–41.
Mascle, J., Martin, L., 1990. Shallow structure and recent evolution of the Aegean Sea: a synthesis based on continuous reflection profiles. Marine Geol. 94, 271–299.
McClusky, S., Balassanian, S., Barka, A., Demir, C., Erginav, S., Georgiev, I., Gurkan, O., Hamburger, M., Hurst, K., Kahle, H., Kastens, K., Kekelidze, G., King, R., Kotzev, V., Lenk, O., Mahmoud, S., Mishin, A., Nadarya, M., Ouzounis, A., Paradissis, D., Peter, Y., Prilepin, M., Reilinger, R., Sanli, I., Seeger, H., Tealeb, A., Toksoz, M.N., Veis, G., 2000. Global Positioning System constraints on plate kinematics and dynamics in the eastern Mediterranean and Caucasus. J. Geophys. Res. 105 (B3), 5695–5719.
McDougall, I., Harrison, T.M., 1999. Geochronology and Thermochronology by the $^{40}Ar/^{39}Ar$ Method. Oxford University Press, Oxford. 269 p.
McNeill, L.C., Mille, A., Minshull, T.A., Bull, J.M., Kenyon, N.H., Ivanov, M., 2004. Extension of the North Anatolian fault into the North Aegean trough: evidence for transtension, strain partitioning, and analogues for Sea of Marmara basin models. Tectonics 23, TC2016. doi:10.1029/2002TC001490.
Mercier, J.L., Sorel, D., Vergely, P., Simeakis, K., 1989. Extensional tectonic regimes in the Aegean basins during the Cenozoic. Basin Res. 2, 49–71.
Mountrakis, D., 2006. Tertiary and Quaternary tectonics of Greece. In: Dilek, Y., Pavlides, S. (Eds.), Postcollisional Tectonics and Magmatism in the Mediterranean Region and Asia: Geol. Soc. Amer. Spec. Pap., 409, pp. 125–136.
Mountrakis, D., Tranos, M., Papazachos, C., Thomaidou, E., Karagianni, E., Vamvakaris, D., 2006. Neotectonic and seismological data concerning major active faults, and the stress regimes of Northern Greece. In: Robertson, A.H.F., Mountrakis, D. (Eds.), Tectonic Development of the Eastern Mediterranean Region: Geol. Soc. Lond. Spec. Publ., 260, pp. 649–670.
Nance, R.D., 1981. Tectonic history of a segment of the Pelagonian zone, northeastern Greece. Can. J. Earth Sci. 18, 1111–1126.
Papanikolaou, D.J., 1984. The three metamorphic belts of the Hellenides: a review and a kinematic interpretation. In: Dixon, J.E., Robertson, A.H.F. (Eds.), The Geological Evolution of the Eastern Mediterranean: Geol. Soc. Lond. Spec. Publ., 17, pp. 551–561.
Papanikolaou, D., 2009. Timing of tectonic emplacement of the ophiolites and terrane paleogeography in the Hellenides. Lithos 108, 262–280.
Papanikolaou, D., Alexandri, M., Nomikou, P., 2006. Active faulting in the north Aegean basin. In: Dilek, Y., Pavlides, S. (Eds.), Postcollisional tectonics and magmatism in the Mediterranean region and Asia: Geol. Soc. Amer. Spec. Pap., 409, pp. 189–209.
Piper, D.J.W., Perissoratis, C., 1991. Late Quaternary sedimentation on the north Aegean continental margin, Greece. Amer. Assoc. Petrol. Geol. Bull. 75, 46–61.
Psilovikos, A., 1984. Phenomena of river incision and terrace formation on the eastern foothills of Mt. Olympus, Greece. Revue de Géographie, Institute de Géographie Académ, Slovaque des Sciences Brataslava, 36, pp. 201–216.
Reilinger, R.E., McClusky, S.C., Oral, M.B., King, R.W., Toksoz, M.N., Barka, A.A., Kinik, I., Lenk, O., Sanli, I., 1997. Global positioning system measurements of present-day crustal movements in the Arabia–Africa–Eurasia plate collision zone: J. Geophys. Res. 102, 9983–9999.
Ricou, L.E., Burg, J.-P., Godfriaux, I., Ivanov, Z., 1998. Rhodope and Vardar; the metamorphic and olistostromic paired belts related to Cretaceous subduction under Europe. Geodin. Acta 11 (6), 2895–3309.
Saatçilar, R., Ergintava, S., Demirbagb, E., Inan, S., 1999. Character of active faulting in the North Aegean Sea. Marine Geol. 160, 339–353.
Schermer, E.R., 1990. Mechanisms of blueschist creation and preservation in an A-type subduction zone, Mount Olympos region, Greece. Geology, 18, 1130–1133.
Schermer, E.R., 1993. Geometry and kinematics of continental basement deformation during the Alpine orogeny, Mt. Olympos region, Greece. J. Struct. Geol. 15, 571–591.
Schermer, E.R., Lux, D.R., Burchfiel, B.C., 1990. Temperature–time history of subducted crust, Mount Olympus region, Greece. Tectonics 9, 1165–1195.
Schmitt, A., 1983. Nouvelles contributions à l'étude géologique des Pieria, de l'Olympe, et de l'Ossa (Grèce du Nord) [Ph.D. dissert.]. Mons, Belgium, Faculté Polytechnique de Mons. 215 pp.
Sharp, I.R., Robertson, A.H.F., 2006. Tectonic-sedimentary evolution of the western margin of the Mesozoic Vardar Ocean: evidence from the Pelagonian and Almopias zones, northern Greece. Geol. Soc. Lond. Spec. Publ. 260, 373–412.
Smith, G.W., Nance, R.D., Genes, A.N., 1997. Quaternary glacial history of Mount Olympus, Greece. Geol. Soc. Amer. Bull. 109, 809–824.
Smith, G.W., Nance, D., Genes, A.N., 2006. Pleistocene glacial history of Mount Olympus, Greece: neotectonic uplift, equilibrium line elevations, and implications for climatic change. In: Dilek, Y., Pavlides, S. (Eds.), Postcollisional Tectonics and Magmatism in the Mediterranean region and Asia: Geol. Soc. Amer. Spec. Pap., 409, pp. 157–174.
Stiros, S., Arnold, M., Laborel, F., Pirazzoli, P., Pomoni-Papaioannou, F., 1994. Late Quaternary uplift of the Olympus–Pelion Range coasts (Macedonia–Thessaly, Greece). Bull. Geol. Soc. Greece 30, 325–330.
Taymaz, T., Jackson, J., McKenzie, D., 1991. Active tectonics of the north and central Aegean sea, Geophys. J. Int. 106, 433–490.
van Hinsbergen, D.J.J., Langereis, C.G., Meulenkamp, J.E., 2005. Revision of the timing, magnitude and distribution of Neogene rotations in the western Aegean region. Tectonophysics, 396, 1–34.
Vergely, P., 1976. Chevauchment vers l'ouest et retrocarriage vers l'est des ophiolites; deux phases tectoniques au cours du Jurassique superior-Eocrétace dans le Hellenides internes. Bull. Soc. Geol. France 18, 233–246.
Yarwood, G.A., Aftalion, M., 1976. Field relations and U–Pb geochronology of a granite from the Pelagonian zone of the Hellenides (High Pieria, Greece). Bull. Soc. Geol. 7 (18), 259–264 France, séries.

View publication stats